NATURAL CONVECTION IN A RECTANGULAR CAVITY WITH INTERNAL HEAT GENERATION

Willy Smith*

Frederick G. Hammitt**

The University of Michigan

Department of Nuclear Engineering

Laboratory for Fluid Flow and Heat Transfer Phenomena

Internal Report 05031-2-I

April 1965.

* Research Associate, Nuclear Engineering Department, The University of Michigan.

** Professor, Nuclear Engineering Department, The University of Michigan.

AKNOWLEDGMENTS

Financial support for the work described in this report was provided by the Michigan Memorial Phoenix Project and the National Science Foundation.

***

1. Introduction

Contributions to the field of natural convection have been relatively limited in recent years, due primarily to the inherent complexity of the applicable non-linear differential equations and the scantiness of important applications. However, high-speed digital computers have made practical the finding of accurate enough numerical solutions, while important applications have come into being both in nuclear reactors and space technology, thus reviving the interest in the subject.

The present work considers a closed rectangular cavity with internal heat generation, cooled along a pair of vertical side walls, and simulating the channels in an internally-cooled homogeneous nuclear reactor. Although the experiment used water, the theoretical analysis considers fluids of arbitrary Prandtl number. A formal relationship between the applicable non-dimensional parameters, following the one-fourth power law typical of natural convection, was obtained. Good agreement between experimental and theoretical results was found.

2. Theoretical Analysis

The conventional fluid flow equations of continuity, Navier-Stokes, and conservation of energy, properly modified to include a heat source term, provide the starting point. The following assumptions are made:

i) the fluid is quasi-incompressible, i.e., the density is constant except for its temperature dependence in the body force per unit mass term, where: $\underline{F} = -g\beta(T-T_o)$.

ii) internal heat dissipation by viscous forces is negligible compared to heat source input.

iii) viscosity, thermal conductivity, and specific heat are constant and evaluated for a conveniently defined mean temperature.

Then*:

$$\operatorname{div} \underline{V} = 0$$

$$\frac{D\underline{V}}{Dt} = -\underline{g}\beta(T-T_o) - \frac{1}{\rho} \operatorname{grad} p + \nu \nabla^2 \underline{V}$$

$$\frac{DT}{Dt} = K\nabla^2 T + \frac{K}{k} Q$$

The x-axis is vertical, and the geometry of the cavity such that one of the horizontal dimensions, z, can be assumed infinite. The equations are normalized by simultaneously making:

$$x = x'b, \qquad y = y'a, \qquad v = v' \frac{K}{a},$$

$$t = t' \frac{a^2}{K}, \qquad u = u' \frac{Kb}{a^2}, \qquad T-T_o = T'(T_m - T_o) = T'\Delta T,$$

$$p = p' \frac{\rho \nu K h^2}{a^4}, \qquad Q = q'\bar{Q} = q' \frac{k\Delta T}{a^2} Nu,$$

where the primes indicate non-dimensional variables, giving[1]:

$$\frac{\partial u}{\partial x} + \frac{\partial v}{\partial y} = 0$$

$$\frac{1}{\sigma}\frac{Du}{Dt} = \frac{a}{b} Ra\, T - \frac{\partial p}{\partial x} + \left(\frac{a}{b}\right)^2 \frac{\partial^2 u}{\partial x^2} + \frac{\partial^2 u}{\partial y^2}$$

$$\frac{1}{\sigma}\frac{Dv}{Dt} = -\left(\frac{b}{a}\right)^2 \frac{\partial p}{\partial y} + \left(\frac{a}{b}\right)^2 \frac{\partial^2 v}{\partial x^2} + \frac{\partial^2 v}{\partial y^2} \qquad (1)$$

$$\frac{DT}{Dt} = \left(\frac{a}{b}\right)^2 \frac{\partial^2 T}{\partial x^2} + \frac{\partial^2 T}{\partial y^2} + q\, Nu$$

where the primes have been dropped for convenience.

Further simplifications are achieved by applying the boundary layer approximation, i.e., assuming the gradients of velocity and temperature in the vertical direction x are small compared to the same gradients in the horizontal direction y. The approximation is improved when $(\frac{a}{b})^2 \ll 1$. The second momentum equation (1) then vanishes, and the remaining equations become:

$$\frac{\partial u}{\partial x} + \frac{\partial v}{\partial y} = 0$$

$$\frac{1}{\sigma}\frac{Du}{Dt} = \frac{a}{b} Ra\ T - \frac{dp}{dx} + \frac{\partial^2 u}{\partial y^2} \qquad (2)$$

$$\frac{DT}{Dt} = \frac{\partial^2 T}{\partial y^2} + q\ Nu$$

Following a procedure similar to Lighthill's[2], although the normalization method is somewhat different, the pressure can be eliminated between eq.(2) and the same equation written at the wall (y = 1), where the boundary conditions are: v = u = 0 (non-slip), and: $T = T_w(x)$, T_w being a known wall temperature distribution. Then, for the steady-state case:

$$\frac{\partial u}{\partial x} + \frac{\partial v}{\partial y} = 0 \qquad (3)$$

$$\frac{1}{\sigma}\left[u\frac{\partial u}{\partial x} + v\frac{\partial u}{\partial y}\right] = \frac{a}{b} Ra(T - T_w) + \left[\frac{\partial^2 u}{\partial y^2}\right]_1^y \qquad (4)$$

$$u\frac{\partial T}{\partial x} + v\frac{\partial T}{\partial y} = \frac{\partial^2 T}{\partial y^2} + q\ Nu \qquad (5)$$

These expressions are still complex. A previously successful method[2-5] is to integrate them across the cavity. Assuming symmetry about the x-axis, i.e., velocity and temperature are even functions, one has:

$$\int_0^1 u\ dy = 0$$

$$\frac{1}{\sigma}\frac{\partial}{\partial x}\int_0^1 u^2 dy = \frac{a}{b}\,Ra\int_0^1 (T - T_w)\,dy + \left[\frac{\partial u}{\partial y} - \frac{\partial^2 u}{\partial y^2}\right]_1$$

$$\frac{\partial}{\partial x}\int_0^1 uT\,dy = \left[\frac{\partial T}{\partial y}\right]_1 + q\,Nu$$

expressing respectively conservation of mass, momentum and energy for the fluid filling each cross section of the vessel.

Following Lighthill[2] again, the second derivative is eliminated by writing eq.(4) at the center line of the cavity ($y = 0$). A term of the form $\frac{1}{\sigma}\,u\left(\frac{\partial u}{\partial x}\right)_{y=0}$ appears, which can be neglected if Prandtl's number is large, or in any case by the boundary layer approximation of small gradients in the x direction, and certainly when the vertical velocity u at the cavity center line is small. The integrated form of the equations is then:

$$\left.\begin{aligned} \int_0^1 u\,dy &= 0 \\ \frac{1}{\sigma}\frac{\partial}{\partial x}\int_0^1 u^2 dy &= \frac{a}{b}\,Ra\int_0^1 (T - T_c)\,dy + \left(\frac{\partial u}{\partial y}\right)_1 \\ \frac{\partial}{\partial x}\int_0^1 uT\,dy &= \left(\frac{\partial T}{\partial y}\right)_1 + q\,Nu \end{aligned}\right\} \quad (6)$$

To this point, the analysis has departed from the classical work of Lighthill[2] only in a different choice of non-dimensional parameters, the inclusion of a non-dimensional heat source term, and the rectangular geometry. A modified Squire's method is used now, whereby temperature and velocity profiles consistent with the boundary conditions are assumed and substituted into eqs.(6). Experimentally and intuitively there is a downward moving boundary layer adjacent to the cooling walls, and an upward moving core. The present experimental data indicate that by and large the core temperature is a function only of vertical

position, i.e., $T_c = T_c(x)$, and in fact, the core is defined here as that region over which the transverse temperature gradient is zero. As substantiated by the experimental data, the temperature profile has a maximum within the boundary layer, and then decreases monotonically toward the wall, as shown in figure 1. A suitable expression for $T(x,y)$ can be shown to be[1]:

$$T(x,y) = T_w + \frac{T_w - T_c}{n(1-d)^3}(y-1)(y^2 + Gy + H) \qquad (7)$$

for $d \leq y \leq 1$, and where:

$$G = G(d) = n(1-d) - 2d$$
$$H = H(d) = n(1-3d+2d^2) + d^2$$

n being a function of d to be determined. For $0 \leq y \leq d$, the temperature is constant; thus:

$$T(x,y) = T_c(x)$$

The present work, then, differs from prior studies[2-5] by the use of this maximum in the temperature profile. Experimental indication of such a maximum had been observed previously by one of the authors in cylindrical geometry[3], but was not incorporated in that analysis. The maximum can be suppressed by making n unity in eq.(7). The profile then reverts to a shape similar to that used in earlier analyses,[2-5] but is not exactly the same, being now a third degree polynomial:

$$T(x,y) = T_w(x) + \frac{T_w - T_c}{(1-d)^3}(y-1)\left[y^2 + (1-3d)y + (1-3d+3d^2)\right]$$

The same general behavior has been previously obtained by a second degree polynomial:[2-5]

$$T(x,y) = T_c(x) + (T_w - T_c)\left(\frac{y-d}{1-d}\right)^2$$

The velocity is assumed constant and positive over the interval $0 \leq y \leq d$, implying equal extent for thermal and frictional boundary layers. Physical arguments justify this assumption[1], although it contradicts an order of magnitude boundary layer analysis. It has been used successfully in preceeding work[2-5], and is also supported by numerical solutions[6] for the flat plate case.

The present data indicate the validity of the above assumption within experimental error. Moreover, the data show that a maximum also exists in the velocity function, as shown in figure 2 (dotted lines). However, the analysis assumes the simpler velocity profile[1] (full line):

$$0 \leq y \leq d : \quad u(x,y) = r(x)$$

$$d \leq y \leq 1 : \quad u(x,y) = r\left\{1 - \left(\frac{y-d}{1-d}\right)^2 \left[1 + s(y-1)\right]\right\}$$

The longer a portion of the fluid remains in a certain location, the more its temperature will be increased because of the internal heat source. It is then reasonable to assume that the location of the temperature maximum and the zero of the velocity function coincide. The relation between n and d is then found to be:

$$n = \frac{19d + 29 - 3\sqrt{3(1-d)(5d+11)}}{16(d+2)}$$

By substitution of u(x,y) into the first of equations (6), an expression for s(d) is found:

$$s(d) = -\frac{4(d+2)}{(d-1)^2}$$

But now there are three unknown functions: d(x), $T_c(x)$, and r(x), with only two equations available. A third equation is obtained[3] by integrating the energy equation (5) over the

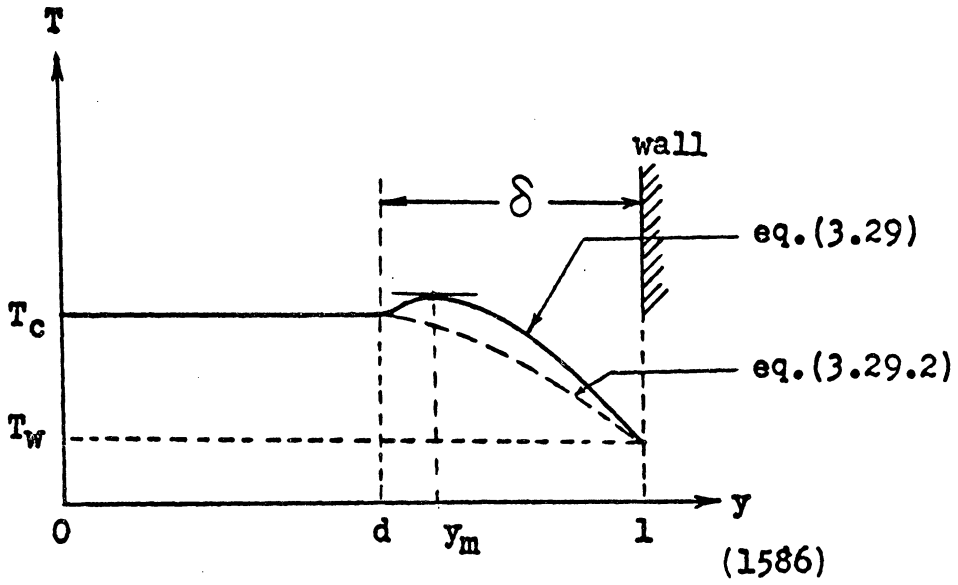

Fig.1. Assumed Temperature Profiles

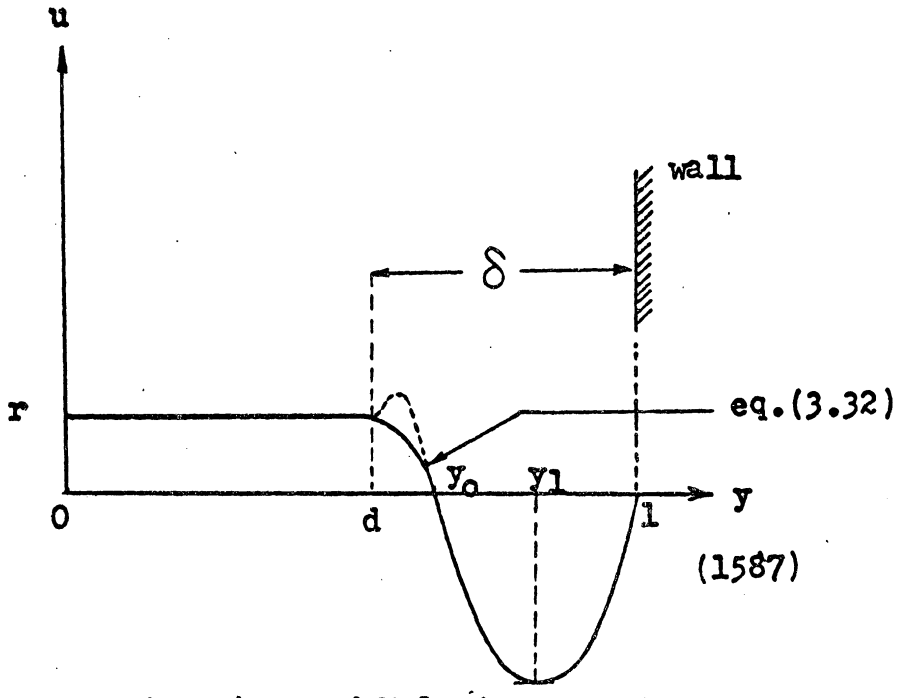

Fig.2. Assumed Velocity Profile

central core only ($-d \leq y \leq d$), and assuming that no fluid is exchanged between core and boundary layer. Then:

$$\frac{\partial}{\partial x}\int_0^d uT\,dy = q\,Nu\,d(x) \qquad (8)$$

Substituting the velocity and temperature profiles into the second and third of equations (6), and into (8), one obtains after considerable amount of algebra:

$$\frac{1}{\sigma}\frac{d}{dx}\left[r^2M(d)\right] = \frac{a}{b}\,Ra(T_w - T_c)P(d) + rR(d) \qquad (9)$$

$$\frac{d}{dx}\left[r(T_w - T_c)N(d)\right] = (T_w - T_c)S(d) + q\,Nu \qquad (10)$$

$$\frac{dT_c}{dx} = \frac{q\,Nu}{r} \qquad (11)$$

where the expressions for the coefficients depend on the temperature profile assumed (see Table I).

These equations must satisfy the following boundary conditions at top and bottom of the cavity:

$$\begin{aligned} T_c(1) = 1, \quad T_c(-1) &= 0 \\ r(\pm 1) &= 0 \\ d(\pm 1) &= 0 \end{aligned} \qquad (12)$$

The first follows from the definition of the non-dimensional temperatures. The second is the non-slip condition, while the third states that the boundary layer thickness must become zero at top and bottom[1,3,4]. This is due to the requirement that at either place the mixed-mean core and boundary layer temperatures must be equal.

The heat distribution q is arbitrary, the strength of the source being proportional to the Nusselt number. However, for the

	Temperature profile characteristics		
	Has maximum $n \neq 1$	No maximum $n = 1$ 3rd. degree polynomial	No maximum 2nd. degree polynomial
M(d)	$\frac{3}{35}\,\frac{d^2 + 11d + 4}{1 - d}$		
N(d)	$\frac{37d+11-56n(2d+1)}{420\,n}$	$-\frac{5d+3}{28}$	$-\frac{2}{15}(1+2d)$
P(d)	$\frac{(1-d)(4n-1)}{12n}$	$\frac{1-d}{4}$	$\frac{1-d}{3}$
R(d)	$\frac{6(1+d)}{(1-d)^2}$		
S(d)	$\frac{1+2n}{n(1-d)}$	$\frac{3}{1-d}$	$\frac{2}{1-d}$

Table I. Coefficients of the basic equations corresponding to the different temperature profiles.

present work, uniform heat distribution was assumed ($q = 1$).

The wall temperature distribution can also be selected arbitrarily, with the only restriction that $T_w(-1) = 0$, which results from the definition of non-dimensional temperature differential. Only linear variations of $T_w(x)$ were considered:

$$T_w(x) = \frac{1}{2m}(x+1) \tag{13}$$

where $m > 1$. The case $m = \infty$ corresponds to constant wall temperature.

3. Numerical Solution

The set of equations (9),(10) and (11) is too complex for analytical treatment, but can be successfully attacked by numerical methods. In the present cases, satisfactory solutions were found using a fourth order Runge-Kutta integration procedure in a 7090 IBM digital computer.

An additional difficulty is that the numerical integration can be started only if a well defined point is known. In the case under analysis, the points $x = \pm 1$ where the values of the functions are given by the boundary conditions (12) are also singular points. This difficulty was circumvented by replacing the differential equations by a set of algebraic equations which will provide an approximate solution valid only in the neighborhood of $x = 1$, the accuracy of this asymptotic solution increasing as $x = 1$ is approached. The resulting equations are still complicated enough to require iteration methods and a computer[1].

For given Prandtl number and specified wall temperature distribution, a value of Ra was selected and a reasonable corresponding value of Nu assumed on the basis of experimental or

previous numerical results. Starting from the top of the cavity, the asymptotic solution, valid only about $x = 1$, is used to determine the initial values in terms of the input parameters Ra, Nu, and m. The Runge-Kutta method is then applied, and progresses toward the bottom of the cavity ($x = -1$). The increments selected for the independent variable x are very small at the beginning of the calculation, as well as when the bottom is approached, and somewhat larger in the middle region. The exactness of the solution is increased with decreasing values of Δx, but by the same token the computing time is increased, so that a suitable compromise must be made.

When the bottom of the cavity is approached, if the boundary conditions (12) are not satisfied within a preset value, the Nusselt number is modified accordingly, and the computation repeated starting again from the top.

Two types of solutions were analysed:

a) Large Prandtl number: Considerable simplification is achieved since the left-hand side of eq.(9) can be altogether neglected. This equation provides then an explicit expression for r(x), which when substituted into (10) and(11),and also using (13), gives a system of two differential equations in two unknowns:

$$\frac{d}{dx}\left[-\frac{a}{b}\,Ra(T_w - T_c)^2\,\frac{P(d)N(d)}{R(d)}\right] = (T_w - T_c)S(d) + Nu$$

$$\frac{d(T_w - T_c)}{dx} = \frac{1}{2m} + \frac{b\,Nu\,R(d)}{a\,Ra(T_w - T_c)P(d)}$$

These equations were numerically solved following the procedure described above, for values of m ranging from 1.5 to 1000. The results, in terms of the non-dimensional parameters, are presented in figure 9 .

b) Arbitrary Prandtl number: The solution for arbitrary values of σ presents greater difficulties. The Runge-Kutta method requires not only knowledge of an initial point , but also that the equations can be cast into the form:

$$d' = f_1(x,d,T_c)$$
$$r' = f_2(x,d,T_c)$$
$$T_c' = f_3(x,d,T_c)$$

where the derivatives with respect to x are expressed as functions of only the dependent variables . This was accomplished after some manipulation[1].

The input parameters for the theoretical solution are the Prandtl number σ, characterizing the fluid, and m, fixing the slope of the imposed linear wall temperature distribution. For each pair of values σ, m, many pairs of corresponding values of the non-dimensional parameters Nu and $\frac{a}{b}$ Ra are calculated, and in each computation, values of the functions d(x), r(x), and $T_c(x)$ across the cavity were obtained. Values of σ considered range from 0.01 to 10.

The results are presented in two ways: i) in terms of the parameter m, for fixed Prandtl number; and ii) for different values of σ and given wall temperature distribution (i.e., fixed m).

For the first case, figures 3, 4, and 5, the curves refer to large σ (≥ 10), and correspond to a constant value of Ra. When the wall temperature has large slope (m = 1.5), the thickness of the boundary layer is quite uniform far from the ends of the cavity, and the core velocity r(x) also remains fairly constant. As the constant wall temperature case is approached ($m \to \infty$), the changes in boundary layer thickness become greater, with

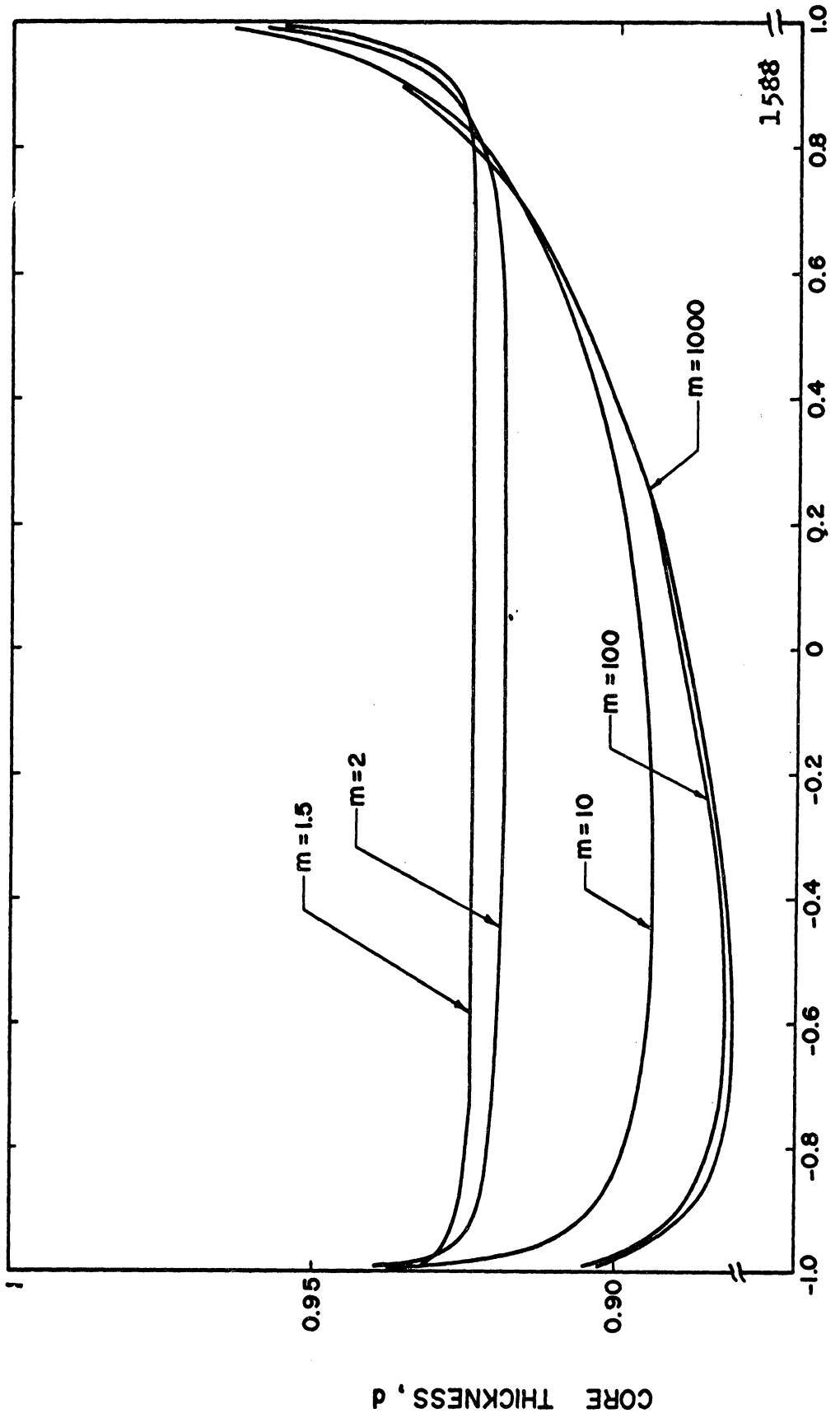

Fig.3. Theoretical core thickness for variable wall temperature distribution and constant Rayleigh number.

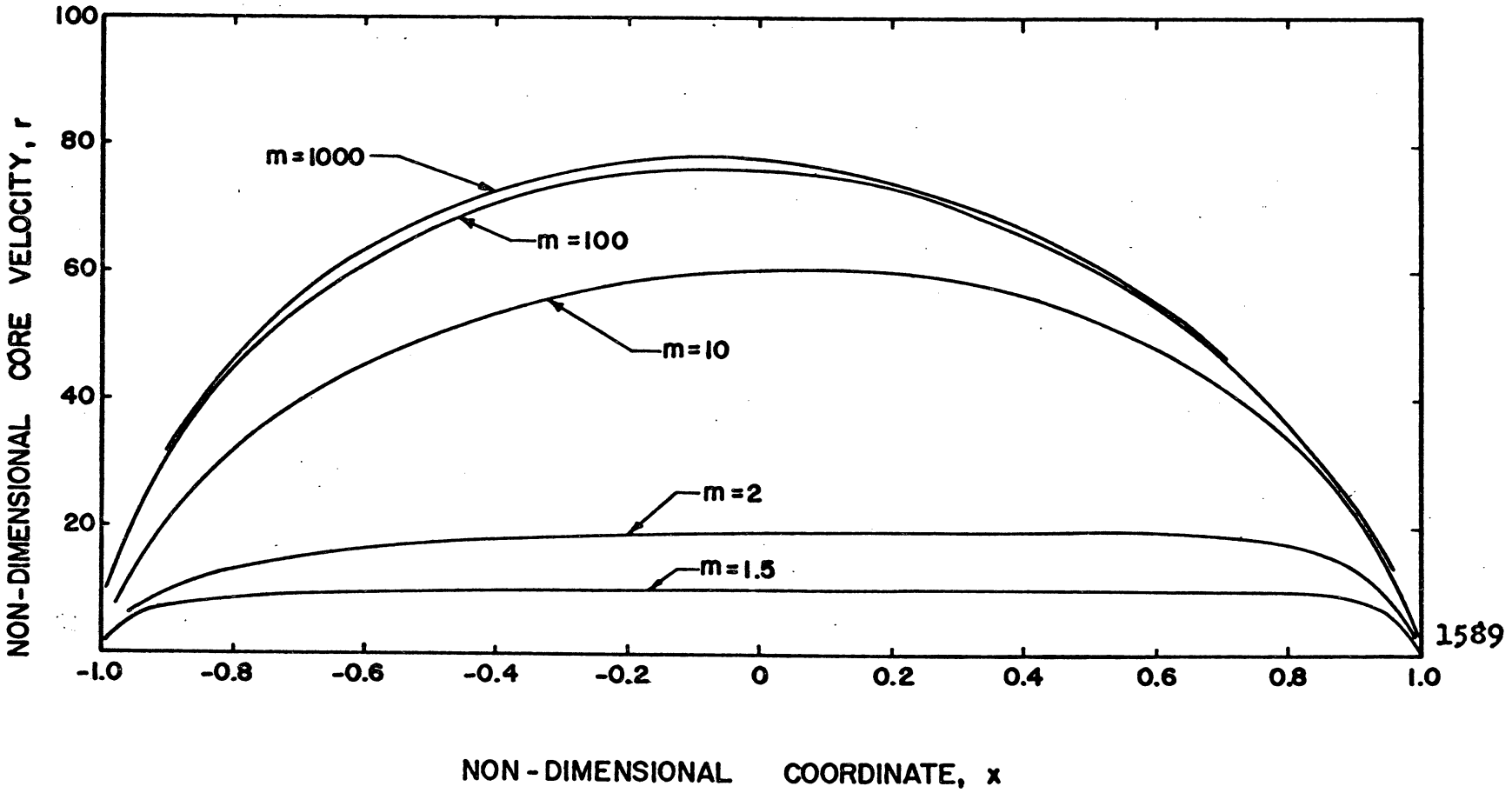

1589

Fig.4. Theoretical core velocity for variable wall temperature distribution and constant Rayleigh number.

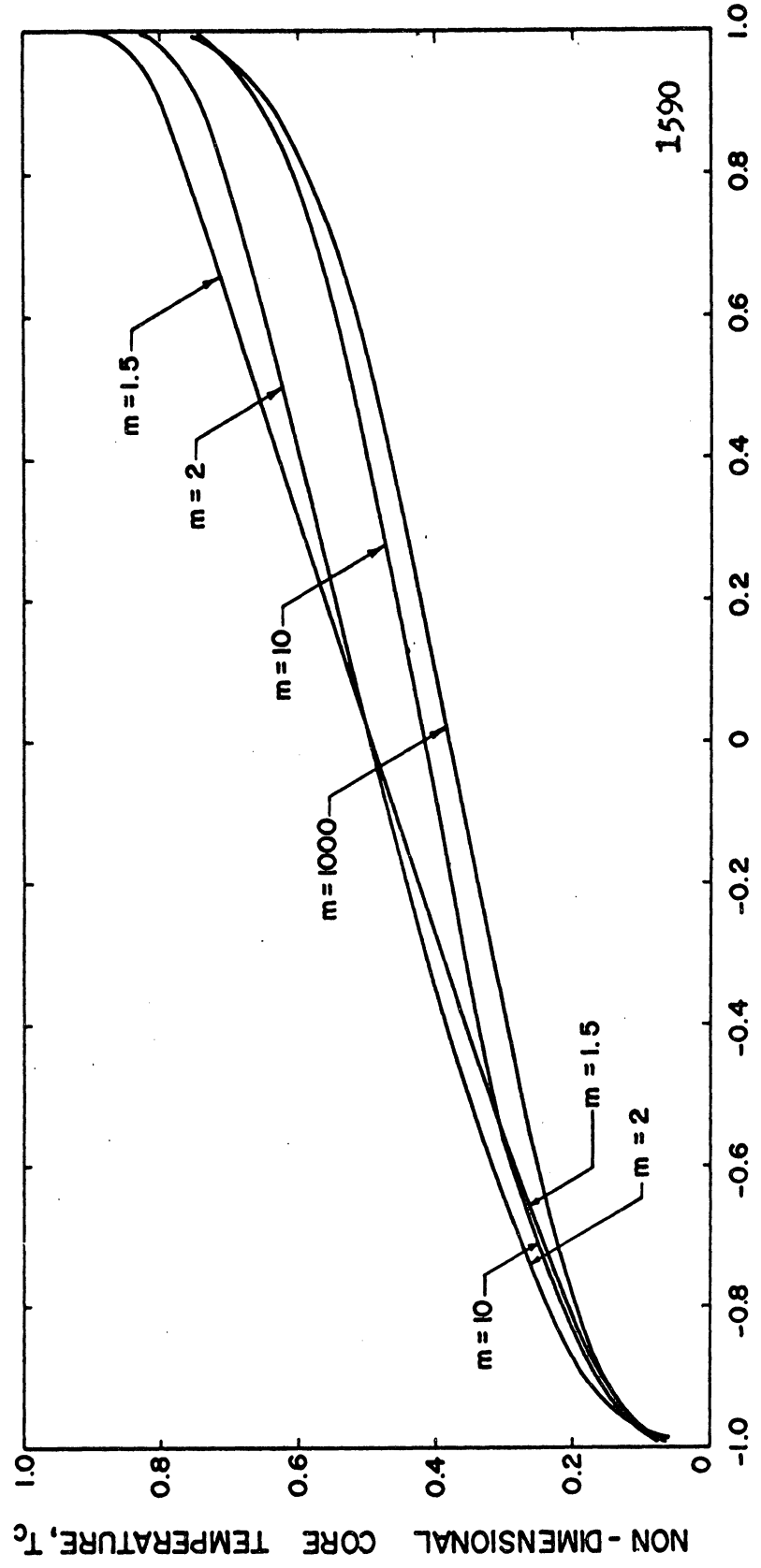

Fig.5. Theoretical core temperature for different wall temperature distribution and constant Ra.

increasing thicknesses appearing toward the bottom of the cavity. Core velocity varies in a similar manner with m, while core temperature is not so sensitive to changes in wall temperature distribution.

In the second set of curves, figures 6, 7, and 8, corresponding to constant wall temperature and fixed Rayleigh number, the boundary layer thickness is rather constant for large σ, although it tends to increase toward the bottom. As σ decreases, the trend reverses and the thicker parts of the boundary layer appear close to the top. Core temperature shows little change for different values of σ.

The following relationship among the non-dimensional parameters was found:

$$Nu = C(m,\sigma)\left(\frac{a}{b}\,Ra\right)^{1/4} \qquad (14)$$

This expression not only verifies that the one-fourth power law, known to be associated with other cases of natural convection, is also valid for the present problem, but also allows easy comparison between the present results and those of other investigators, as shown in fig.9.

Theoretical results by Chu[5] indicate that Lighthill's[2] "large" value of σ is about 10, and for this value their solutions coincide. Chu's solutions cover the range $0.02 \leq \sigma \leq 10$, and apply to cylindrical geometry similar to Lighthill's,* but there is no internal heat generation.

Previous work by Hammitt[3,4,7] was performed in closed cylindrical geometry with internal heat generation. The

---

* Cylinder with reservoir on top.

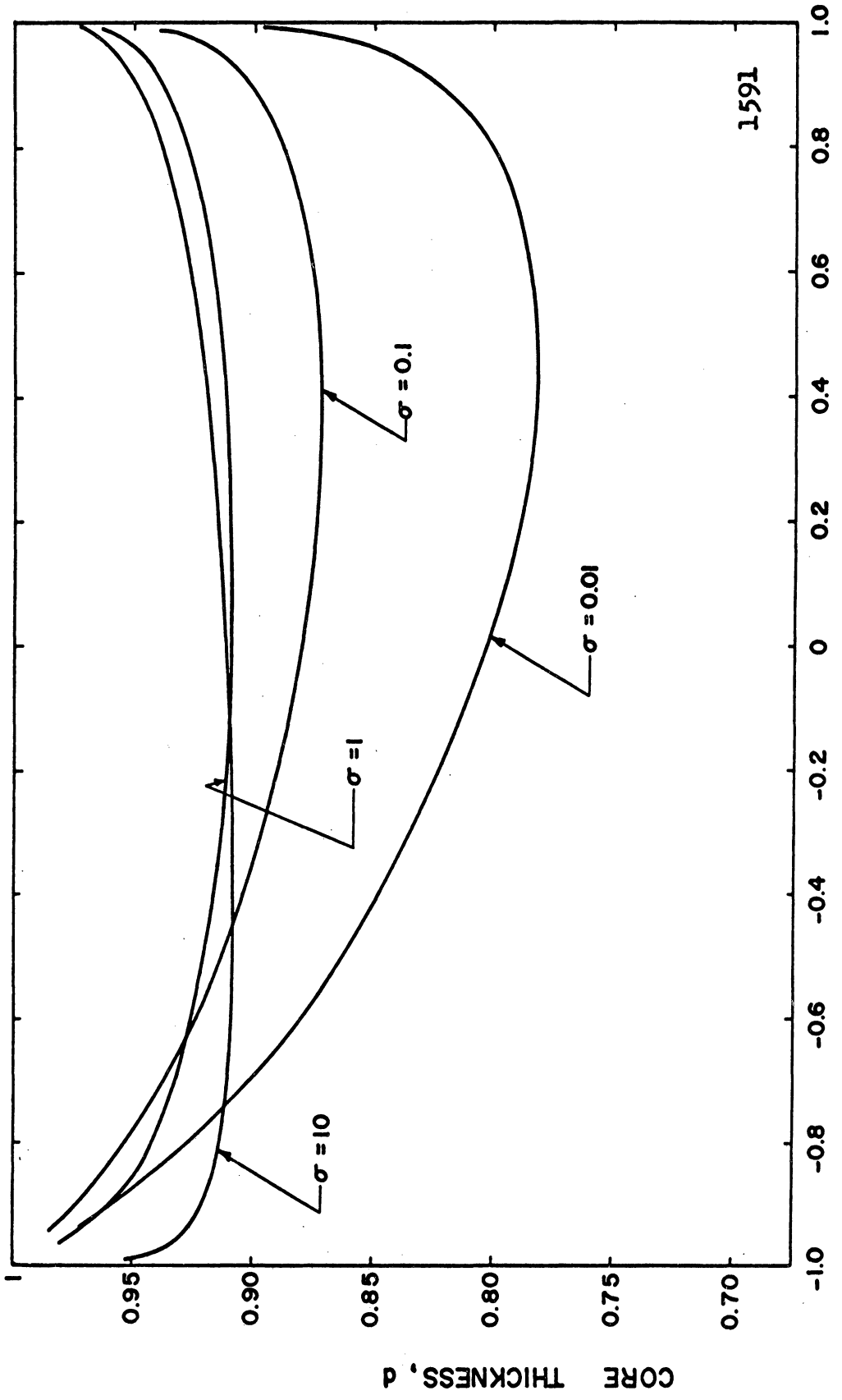

Fig.6. Theoretical core thickness as obtained from the general solution for variable σ, constant Ra and constant wall temperature.

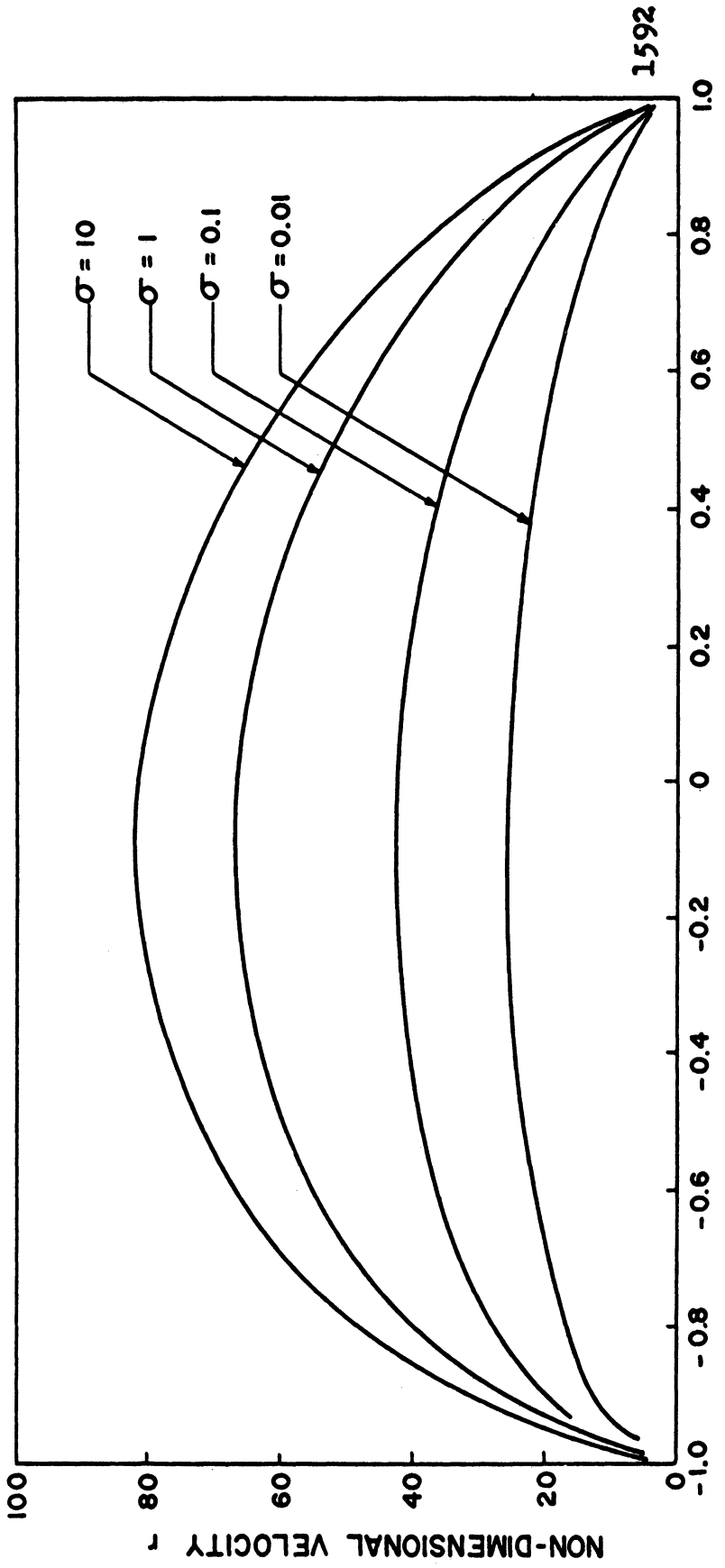

Fig. 7. Theoretical core velocity as obtained from the general solution for variable σ, constant Ra and constant wall temperature.

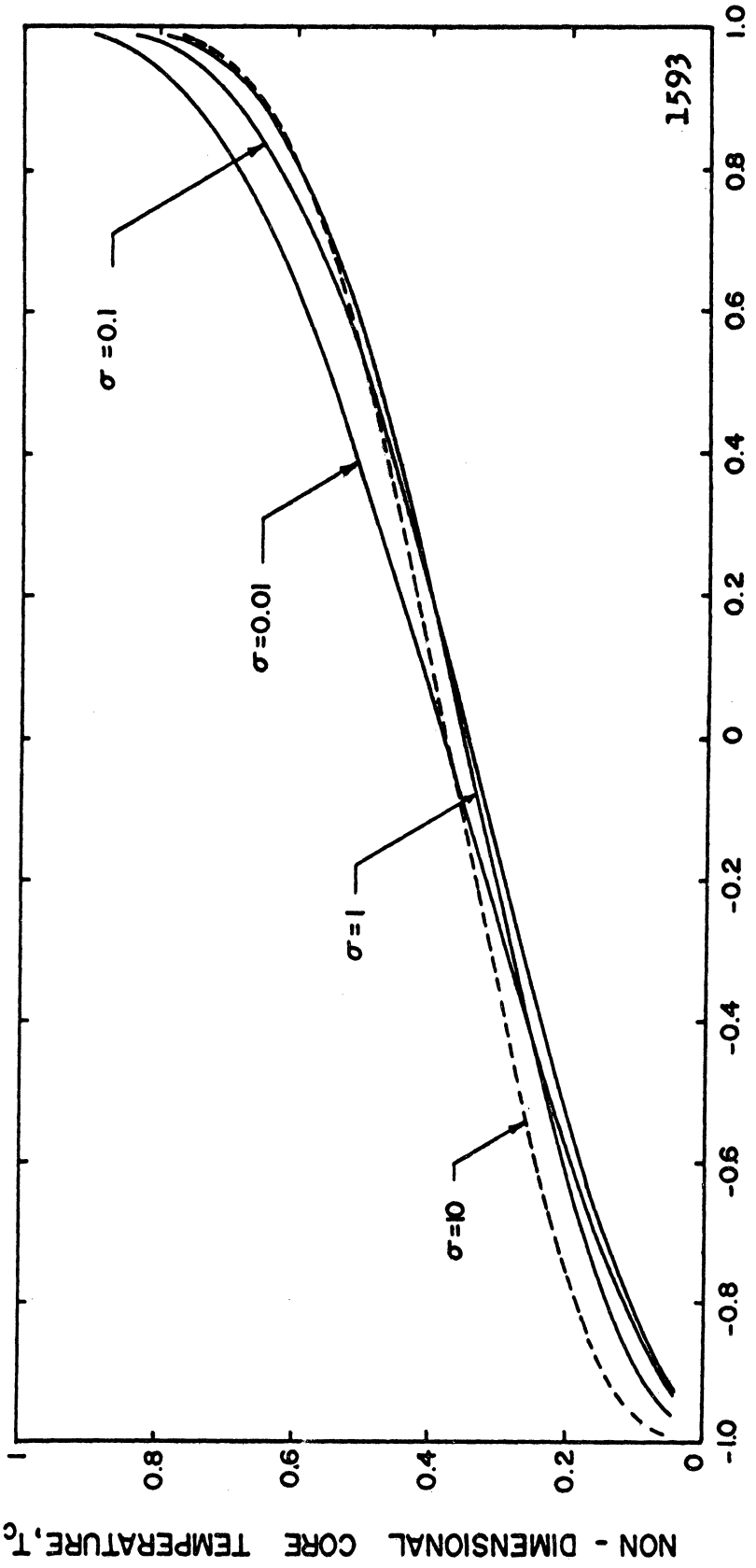

Fig.8. Theoretical core temperature as obtained from the general solution for variable σ, constant Ra and constant wall temperature.

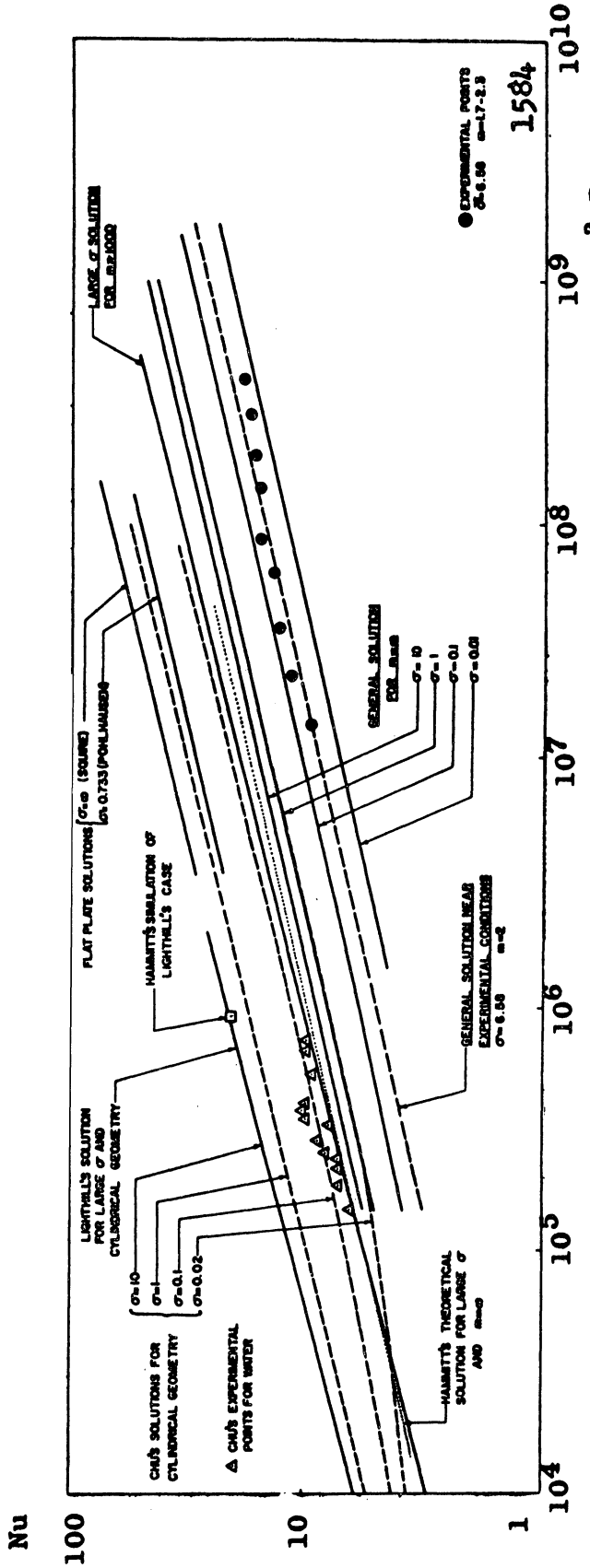

Fig.9. Summary of theoretical and experimental data.

theoretical solution for large σ agrees well with the solution found in the present work also for large σ . For a given $\frac{a}{b}$ Ra value, both solutions show lower Nu than those found by Chu[5]. Since the Chu and Lighthill solutions are in agreement, and Hammitt reproduced Lighthill's results in a closed geometry by assuming the heat source to be an infinitely thin disc at the bottom of the cavity, it appears that the reduction in Nu is due to the inclusion of the volumetric heat source. Solutions for closed cylindrical and rectangular geometries are almost coincident, indicating relative independence on geometry.

Present theoretical results for large and arbitrary Prandtl number are also shown in fig.9. The solutions are for constant wall temperature. For $\sigma > 10$, the lines are almost coincident, althpugh the solution for $\sigma = 10$ is still below that obtained for "large" Prandtl number. This discrepancy results from the use of different temperature profiles: for the large σ solution, a simplified temperature profile was used, while for the arbitrary Prandtl number solution a temperature profile with a maximum was assumed, in accordance with the experimental observations. Thus, significant changes in the results have been brought about by the adoption of this more realistic temperature profile.

Values of the coefficient $C(m, \sigma)$ appearing in equation (14) have been calculated for different σ and various wall temperature distributions, as summarized in Table II.

m	σ					
	0.01	0.1	1	6.58	10	∞*
1.42						.1305
1.44						.1338
1.47						.1404
1.48						.1417
1.50				.1073		.1445
1.52						.1490
1.55						.1539
1.58						.1593
1.62						.1654
1.63						.1665
1.78				.1344		
1.86				.1411		
1.95				.1482		
2.00				.1537		.2072
2.02				.1539		
2.10				.1585		
2.20				.1636		
2.25				.1669		
3.50						.2693
5.00				.2286		
10				.2521		.3215
100				.2732		.3344
$\geq$1000	.1208	.1820	.2585	.2815	.2863	.3449

$C(m, \sigma)$.

* correspond to the solution for "large" Prandtl number.

4. Experimental Results

A schematic and a photograph of the experimental facility designed to verify the theoretical treatment are shown respectively in figures 10 and 11. Essentially, it consists of a rectangular cavity (24" high, 8" wide, 36" long) closed at top and bottom and at the smaller vertical sides by plexiglas plates. The larger vertical walls are 1/4" thick brass plates. An A.C. voltage applied across these plates results in heat generation in the cavity due to ohmic resistance. Heat is removed from the cavity through the same brass plates, which are also the interior walls of two vertical cooling tanks. The fluid used was tap water, which provided sufficient electric resistivity for the purpose.

An L-shaped probe electrically insulated from the fluid except at the tip where a small thermocouple bead is located, is inserted through the plexiglas top. I_t can be moved vertically and/or rotated to reach points from the wall to beyond the center line and from top to bottom. The position of the tip of the probe, in terms of non-dimensional distance, can be estimated with an error not larger than $\pm$ 0.01.

A complete temperature mapping of the cavity at power levels ranging from 2.2×10^{-3} to 4.3×10^{-2} watts/cm^3 was obtained. All temperature measurements, more than 2000 in number, were very consistent and reproducible, and were obtained with a precision of the order of $\pm$ 0.05°F. Fig.12 shows typical experimental results corresponding to $Q = 1.02 \times 10^{-2}$ watts/cm^3. The temperature profiles were found to have in all cases the shape assumed for the theoretical

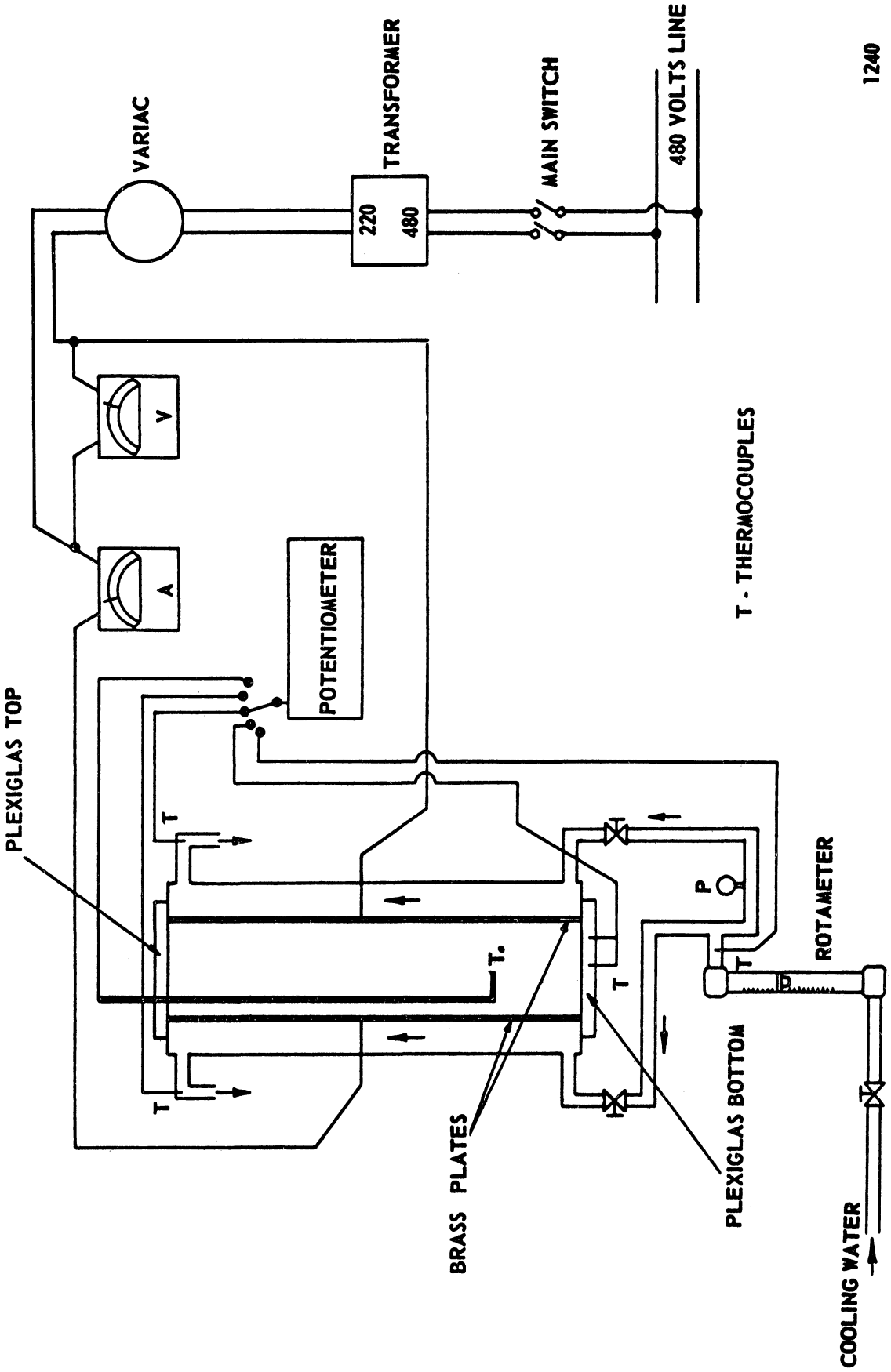

Fig.10. Schematic of rectangular geometry natural convection facility.

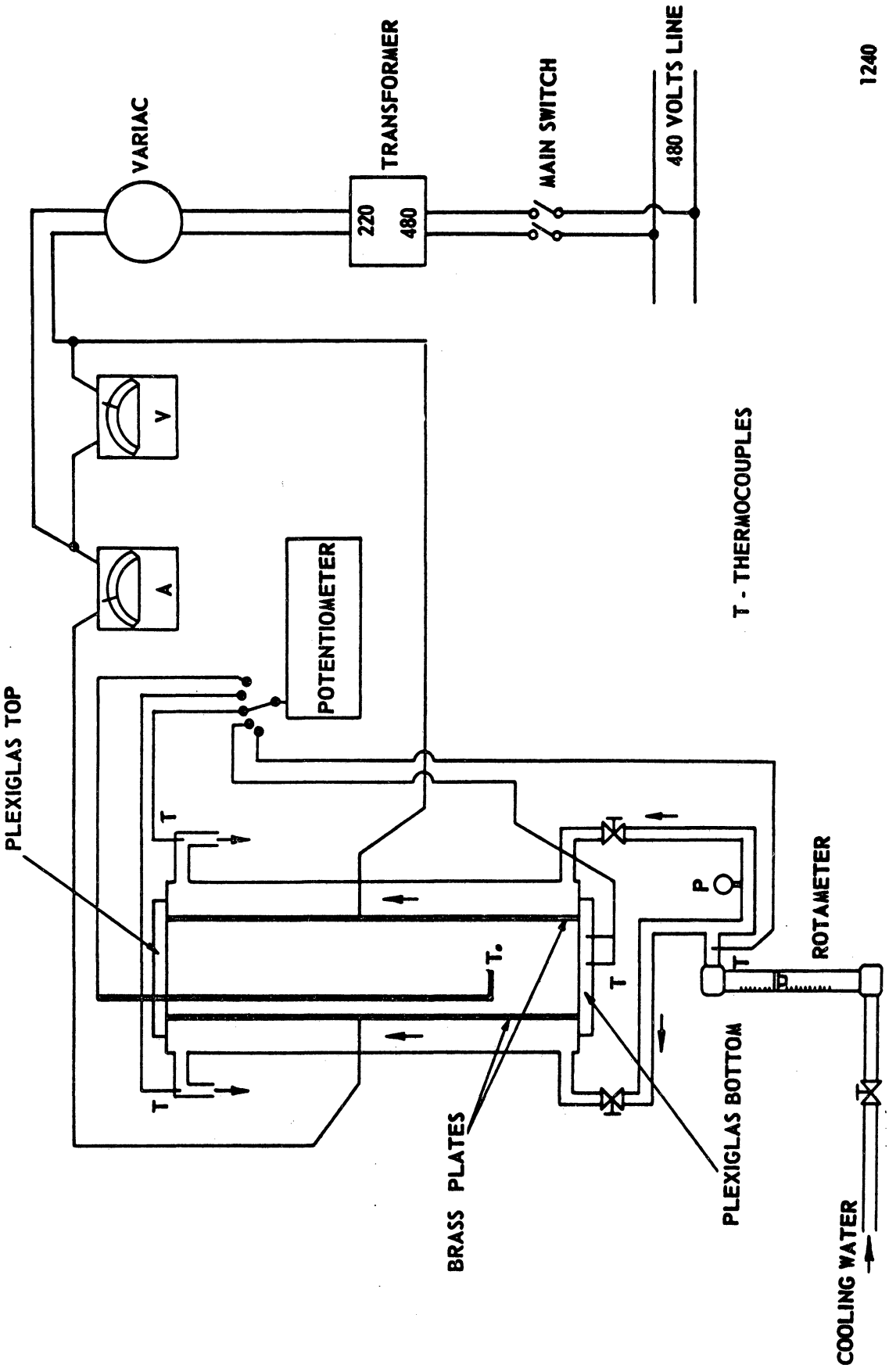

Fig.10. Schematic of rectangular geometry natural convection facility.

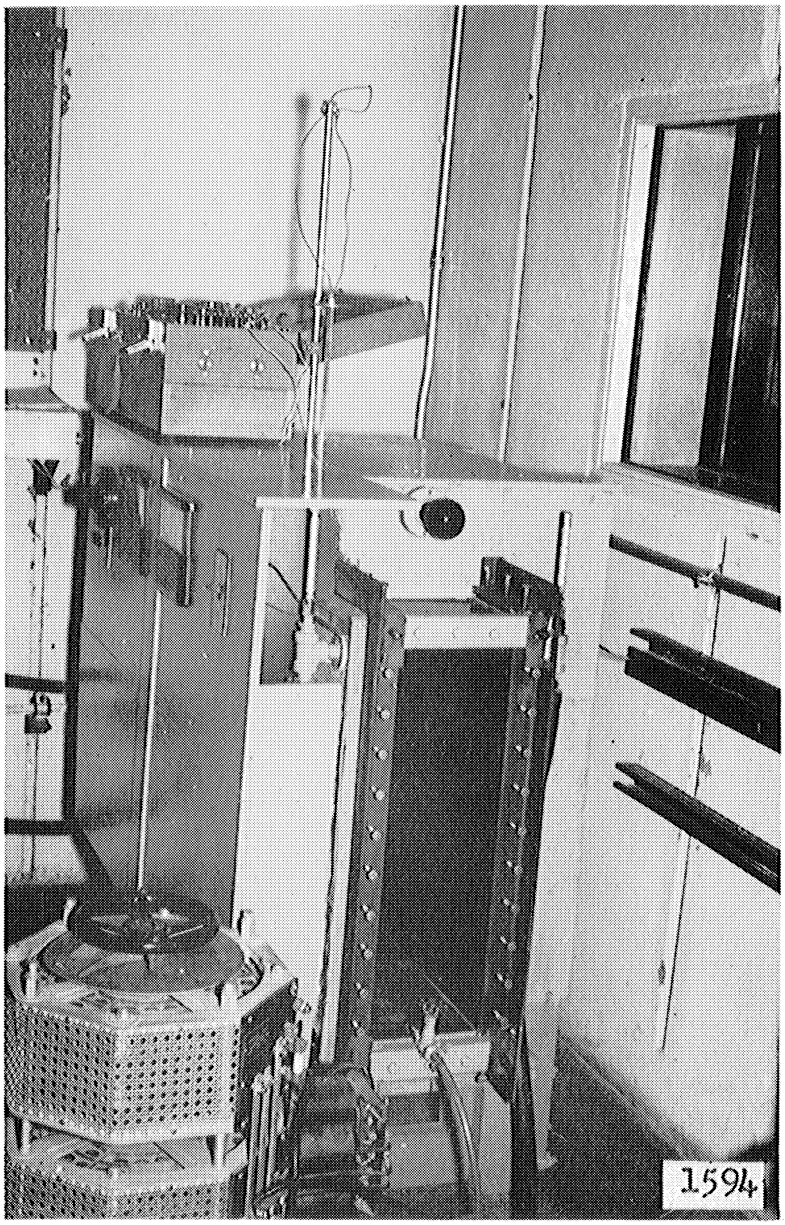

Fig.11. View of the facility.

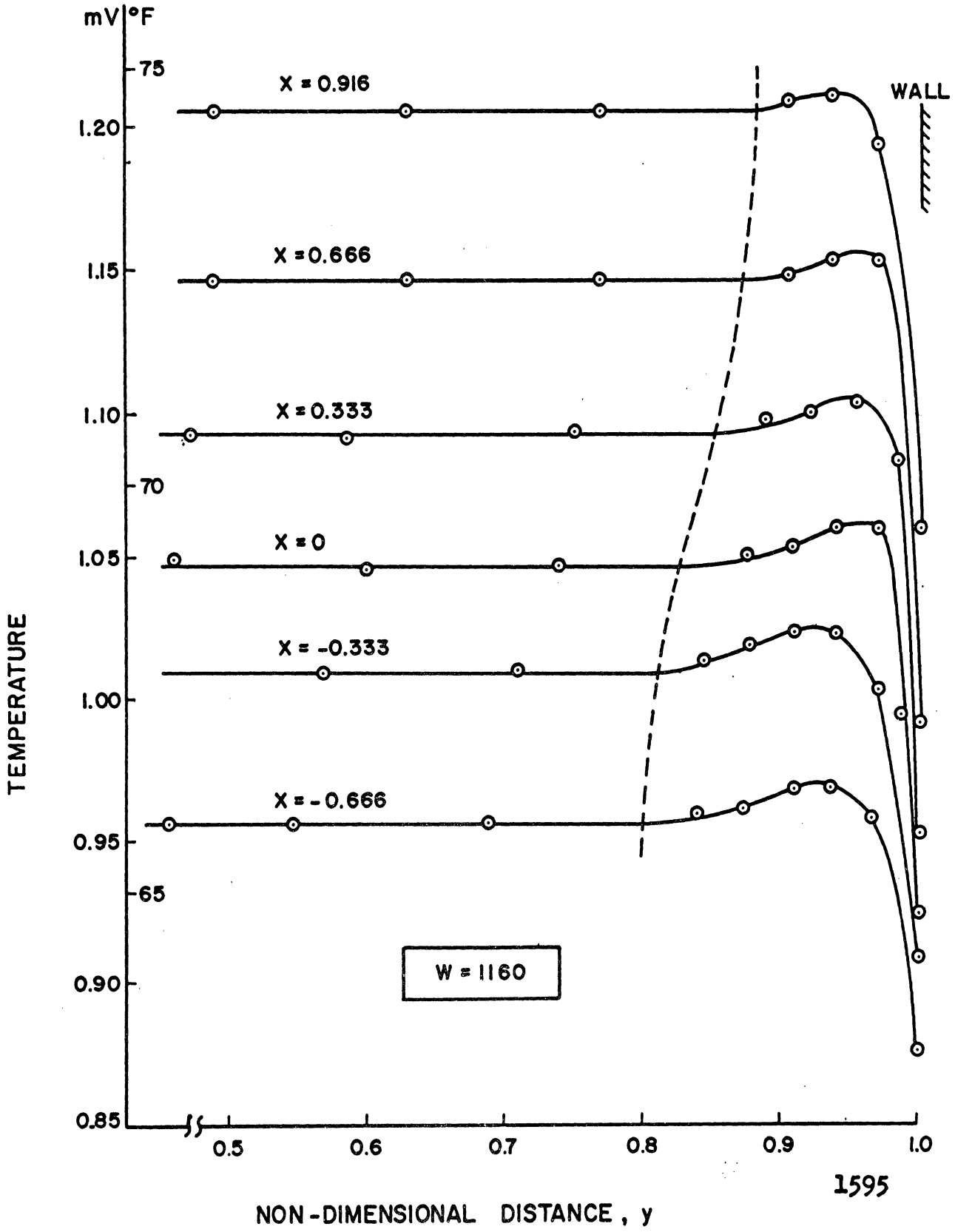

Fig.12. Experimental temperature profiles for a power level of 1.02×10^{-2} watts/cm^3.

analysis, showing a distinct maximum within the boundary layer region.

Curves $T_c(x)$ for each power level were obtained, and are presented in fig.13, where the range of variation at a given position has been indicated with a short vertical line, and a single curve drawn across those lines. Non-dimensional core temperature at all power levels are practically coincident, and compare well with the theoretical curve, thus supporting the underlying theory.

Semi-quantitative velocity measurements were performed by injecting a tracer into the cavity using a similar L-shaped probe terminated in a hypodermic needle. Although these measurements are not so precise as the temperature results, they do compare well with results obtained by a completely separate experimental method (explained below) and with the values resulting from the theoretical analysis.

Fig.14 shows a typical velocity profile obtained by the injection method. Similar plots corresponding to other power levels also show unquestionably the existence of a positive maximum within the boundary layer and adjacent to the core, which has not been previously reported in the literature. All the theoretical analyses[1-5] have been performed using a velocity profiles without that maximum.

The second method of study of the velocity field consisted of taking photographs at equally set time intervals, after small amounts of dye had been injected into the flow. From these photographs, velocities were estimated and found to compare well with the values already obtained by direct timing of the

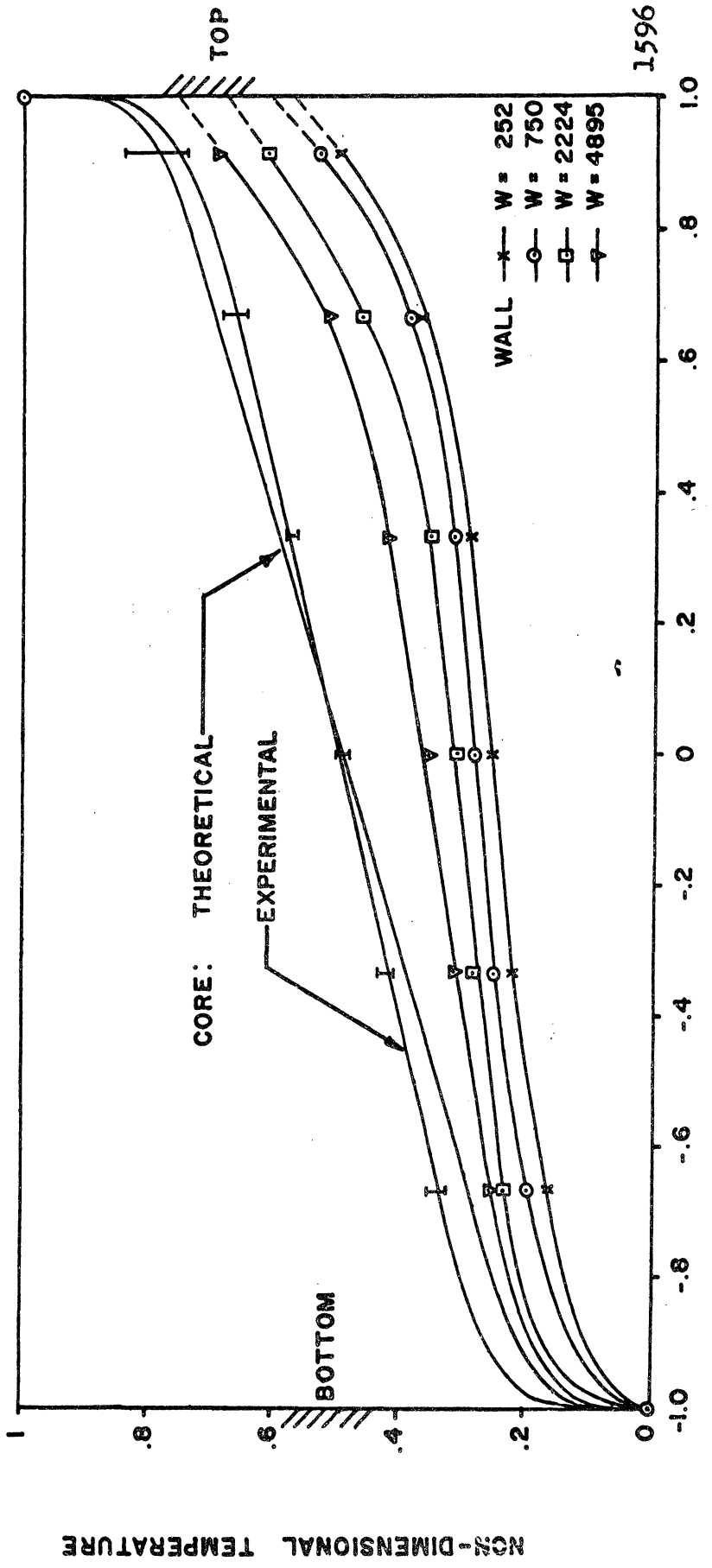

Fig.13. Experimental core and wall non-dimensional temperatures at different power levels.

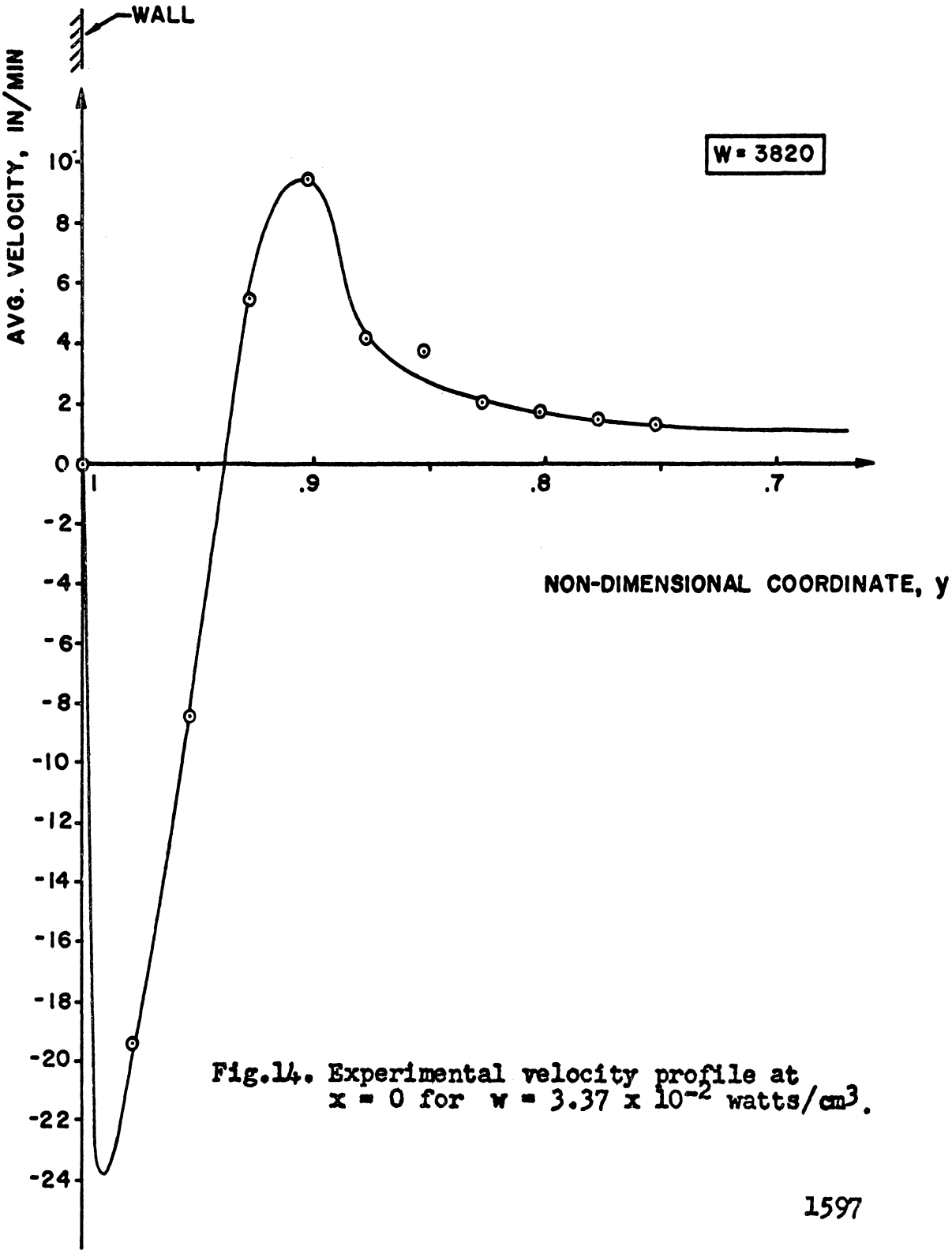

Fig.14. Experimental velocity profile at $x = 0$ for $w = 3.37 \times 10^{-2}$ watts/cm^3.

1597

dye motion. The photographs provide a permanent record of the fluid motions, and show how these are affected by power level. The sequence of photographs in Fig.15* were taken at a power level of 6.6×10^{-3} watts/cm^3, and show that the flow is esentially laminar throughout. In the boundary layer region, some very slow eddying is observed near the bottom of the cavity, while during the same time interval the small amounts of dye injected in the core region have moved upwards without losing their identity. As the power level is increased, some slow eddying appears in the core near the top of the cavity, as shown clearly in fig.16**, corresponding to a power level of 1.96×10^{-2} watts/cm^3, and as also detected by small fluctuations of large period (about 20 sec.) observed in connection with the temperature measurements. Another effect of the increase in the value of the heat source is to sharpen the maximum in the velocity profile.

Values of σ, Nu and $\frac{a}{b}$ Ra were obtained at each power level. Since σ is temperature dependent, and the average temperature within the cavity varies with power level, σ was found to range from 5 to 8, with an average value of 6.58. The other input parameter of the problem, i.e., wall temperature distribution, is also a function of power level. However, for all power levels, $T_w(x)$ shows a linear variation for the middle part of the cavity (see Fig.10), in agreement with the theoretical assumptions. The corresponding values of m range from 1.75 to 2.25. Consequently, all experimental conditions are approximated if the theoretical input parameters are selected to be $\bar{\sigma} = 6.58$ and m = 2. A computer calculation with these values was performed, and the agreement between experimental and theoretical results is excellent (see Fig.9). This good correlation is

(*) $\sigma = 7.53$, Ra = 1.15×10^8, Nu = 13.3
(**) $\sigma = 6.22$, Ra = 4.33×10^8, Nu = 16.4

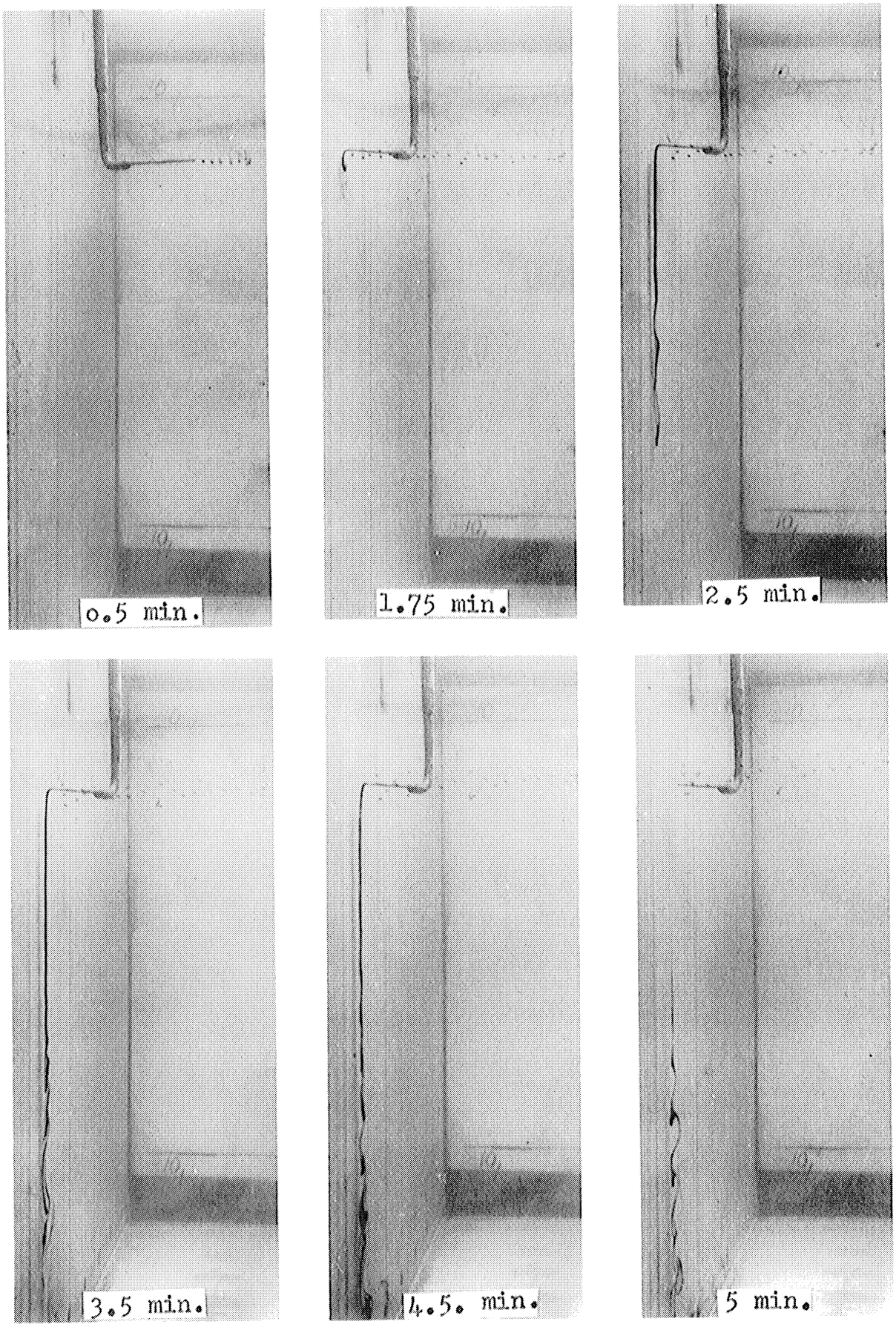

1598

Fig.15. Velocity measurements at a power level of 6.6×10^{-3} watts/cm^3.
$\sigma = 7.53$, Nu = 13.3, Ra = 1.15×10^8.

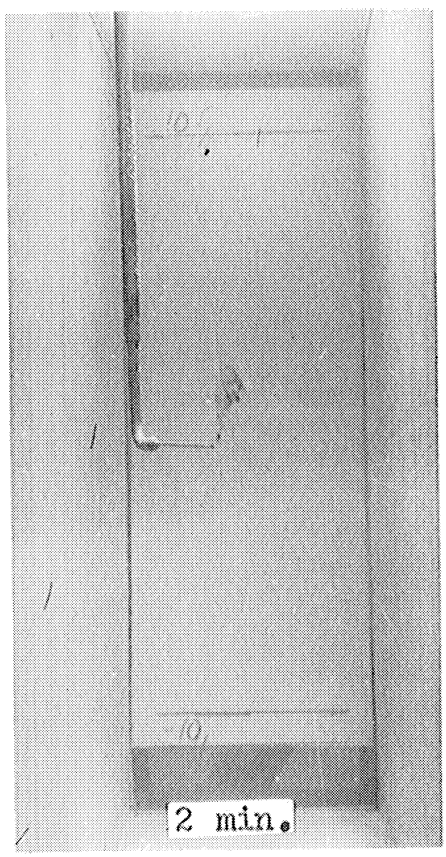

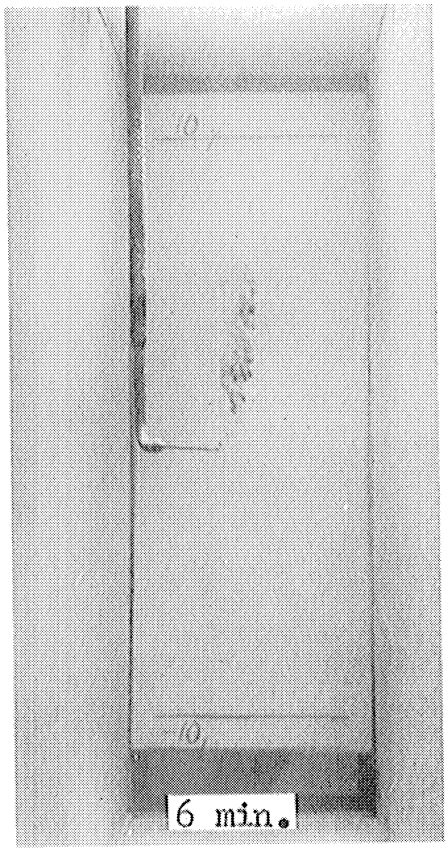

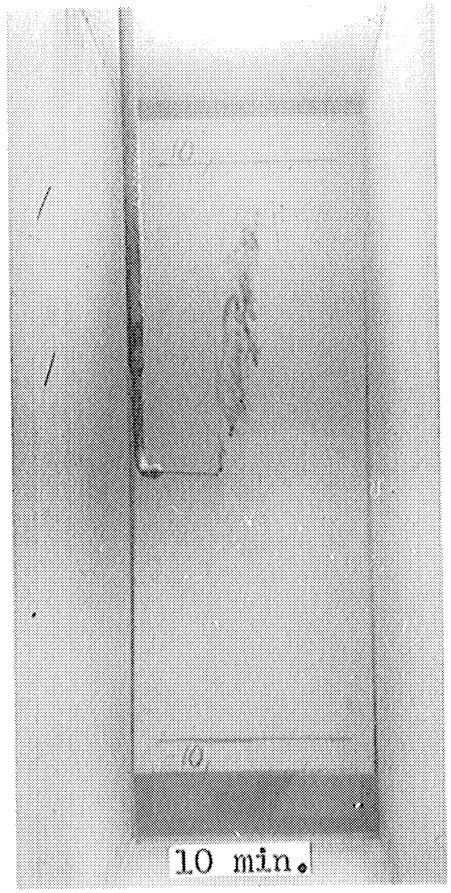

1599

Fig.16. Velocity measurements at a power level of 1.96×10^{-2} watts/cm^3.
$\sigma = 6.22$, Nu = 16.4, Ra = 4.33×10^8.

unexpected, since previous work[3] in a closed cylindrical cavity with internal heat generation, as well as a study[5] in a cylinder with an infinite reservoir on top and no heat source, showed discrepancies between theory and experiment. These discrepancies, small when the fluid was water[3,5] but large for the case of mercury[5], were attributed to turbulence, which existing in the actual experiment was not taken into consideration by the theory. An experimental check of Lighthill's geometry by Martin and Cohen[8] did show good agreement for flow presumably in the laminar regime. In the present work, the observed turbulence was very slight[1]. Thus, the good agreement tends to verify that the previous differences were due mainly to unaccounted turbulent effects.

5. Conclusions

Natural convection flow in a closed cavity has been studied both theoretically and experimentally. The theoretical analysis follows the general lines of Lighthill's procedure, but differs from previous work[1-5] by considering arbitrary values of the Prandtl number, as well as by the following aspects: internal heat generation in rectangular geometry, and temperature profiles with a maximum. Extensive computer calculations verified the existence of a relation (14) among the non-dimensional parameters that follows the one-fourth power law.

The experimental program produced data in good agreement with the theoretical analysis. The temperature mapping indicates that a maximum in the temperature profile exists as assumed, while the velocity results reveal that also the velocity profile has a positive maximum, heretofore not reported. The flow was

found to be esentially laminar up to $\frac{a}{b}$ Ra $\cong$ 4.0 x 10^8, although for values of $\frac{a}{b}$ Ra larger than 2.9 x 10^8 some slow eddying appears in the upper part of the rising central core and in the lower part of the boundary layer.

******

BIBLIOGRAPHY

1. Willy Smith, "Natural Convection in a Rectangular Cavity", Ph.D. Thesis, Nuclear Engineering Dept., The University of Michigan, 1964.

2. M. J. Lighthill, "Theoretical Considerations on Free Convection in Tubes", Quart. Journal Mech. and Applied Math., Vol.VI, Pt.4, 1953, pp.398-439.

3. F. G. Hammitt, "Free Convection Heat Transfer in a Closed Cylindrical Tube with Internal Heat Generation", Ph.D. Thesis, Nuclear Eng. Dept., The University of Michigan, 1957. Also available as Industry Program Report IP-259, The University of Michigan.

4. F.G. Hammitt, E. M. Browre and P. T. Chu, "Free Convection Heat Transfer and Fluid Flow in Closed Vessels with Internal Heat Source", Industry Program Report IP-399, The University of Michigan. Also available as NP-8780, UC-34, O.T.S., Dept. of Commerce, Washington, D.C.

5. P. T. Chu, "Natural Convection Inside a Circular Cavity", Ph.D. Thesis, Dept. of Mech. Engineering, The University of Michigan , 1961.

6. Simon Ostrach, "An Analysis of Laminar Free-Convection Flow and Heat Transfer About a Flat Plate Parallel to the Direction of the Generating Body Force", NACA TN 2635, February 1952.

7. F. G. Hammitt, " Modified Boundary Layer Type Solution for Free Convection Flow in Vertical Closed Tube with Arbitrarily Distributed Internal Heat Source", ASME Paper No.58-SA-30, 1958; abstracted Mech. Engineering 8, No.8, Aug. 1958.

8. B. W. Martin and H. Cohen, " Heat Transfer by Free Convection in an Open Thermosyphon Tube", J. of App. Phys. (London), 5, March 1954.

ws/65